

Rendering along the Hilbert Curve

Alexander Keller, Carsten Wächter, and Nikolaus Binder

Abstract Based on the seminal work on Array-RQMC methods and rank-1 lattice sequences by Pierre L’Ecuyer and collaborators, we introduce efficient deterministic algorithms for image synthesis. Enumerating a low discrepancy sequence along the Hilbert curve superimposed on the raster of pixels of an image, we achieve noise characteristics that are desirable with respect to the human visual system, especially at very low sampling rates. As compared to the state of the art, our simple algorithms neither require randomization, nor costly optimization, nor lookup tables. We analyze correlations of space-filling curves and low discrepancy sequences, and demonstrate the benefits of the new algorithms in a professional, massively parallel light transport simulation and rendering system.

Key words: Quasi-Monte Carlo methods, Hilbert curve, Array-RQMC, low discrepancy sequences, rank-1 lattice sequences, image synthesis.

1 Introduction

In photorealistic image synthesis by light transport simulation, the colors of each pixel are an integral of a high-dimensional function. While the functions to integrate are square-integrable and hence of finite energy, they contain discontinuities that cannot be predicted efficiently. In practice, the pixel colors are estimated by Monte Carlo and quasi-Monte Carlo methods sampling light transport paths that connect light sources and cameras and summing up the contributions.

As a consequence of sampling, images appear noisy when the number of samples is insufficient. This is quite common, when images need to be synthesized rapidly for real-time applications and when convergence is slow due to the intricacies of the

Alexander Keller e-mail: akeller@nvidia.com · Carsten Wächter e-mail: cwachter@nvidia.com · Nikolaus Binder e-mail: nbinder@nvidia.com
NVIDIA, Fasanenstr. 81, 10623 Berlin, Germany

functions to integrate. Depending on the characteristics of the noise in the image, filtering may efficiently improve image quality.

The success of image compression algorithms and compressive sensing methods clearly indicates that the pixels of an image are not independent integrals. One way to account for the correlation of pixels is to consider image synthesis an integro-approximation problem [12].

In this article we propose a new way of synthesizing images as a sequence of correlated integrals such that noise is less perceivable by the human visual system. We therefore review the state of the art in addressing perceived image error in computer graphics in Sect. 2 and introduce our new deterministic algorithm for image synthesis by enumerating a low discrepancy sequence along the Hilbert Curve in Sect. 3. We then explore extensions for progressive image synthesis in Sect. 4 and discuss the results in Sect. 5 before drawing the conclusions.

For the scope of our article, it is sufficient to understand that the mapping of a vector of the low discrepancy sequence to a light transport path is the same across all discussed methods and that methods only differ in which vector of a low discrepancy sequence is assigned to what pixel. This abstraction allows for reproducing the results. For the experiments, we use the Iray light transport simulation and rendering system [19]. For the details we refer to [15, 19, 4, 7] and extensive background information in [27]. A recent survey of sampling methods in computer graphics is [17], while the latest research focuses on low discrepancy sequences with good low-dimensional projections [26, 25].

2 Visual Error in Image Synthesis

The human visual system is quite capable of recovering information from noisy images and computer graphics has been taking advantage of that since its early days [5]. Using the same set of samples across the pixels to synthesize an image may result in disturbingly visible aliasing artifacts. Hence, inspired by the arrangement of receptors in a monkey’s retina [30], a huge body of work around sampling patterns with blue noise characteristics emerged. Especially at low sampling rates and in low dimensions, these patterns have been attractive since they are close to the ideal of reconstructing precisely as long as the assumptions of the sampling theorem are fulfilled, while aliases are mapped to noise, which is very amenable to the human visual system.

For long, an important detail had not been considered explicitly: blue noise characteristics of samples do not matter much for a single pixel integral but when observing an ensemble of neighboring pixels. Only recently, it was found that optimizing the parameters of a Cranley-Patterson rotation per pixel applied to one generic set of samples can dramatically improve the perceived image quality although the ℓ^2 -error remains about the same [10]. Subsequent work extends the optimization to scramblings of the Sobol’ sequence [13]. The visual improvements have been attributed to blue noise characteristics.

Since the ℓ^2 -error between a reference image and different sampling schemes remains about the same, the improvement in perceived image quality must be in the distribution of the error and how the samples are correlated across the pixels [2].

Based on the family of Array-RQMC methods [21] introduced by Pierre L’Ecuyer, we propose simple deterministic quasi-Monte Carlo algorithms that result in similar visual improvements without optimization. In addition, an explanation for the improvements beyond blue noise characteristics is offered. Our approach benefits from the improved uniformity of low discrepancy sequences observed when simulating Markov chains [29, 21] by ordering their states by proximity in world space. Instead of sorting, we explore orders provided by space filling curves in screen space.

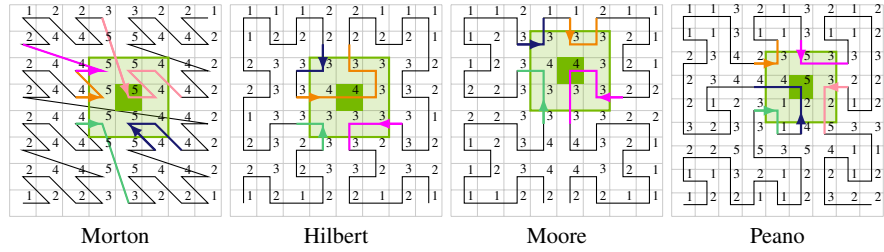


Fig. 1 The Morton, Hilbert, Moore, and Peano space-filling curves on a pixel grid. As the Hilbert, the Moore, and the Peano curve only pass through neighboring pixels, they realize shortest routes of visiting all pixels in the sense of the Traveling Salesman problem. The pixels highlighted in dark green exemplify the number of segments (colored) of each space-filling curve entering the 3×3 neighborhood. This number of segments is depicted for each pixel and its maximum is smallest for the Hilbert and Moore curves. Enumerating the a low discrepancy sequence along a space filling curve, a smaller number of segments implies longer contiguous segments of the low discrepancy sequence used in the 3×3 neighborhood, which improves uniformity.

3 Enumerating Pixels along the Hilbert Curve

Given the resolution of an image to synthesize, a deterministic low discrepancy sequence, and a number of samples to be drawn per pixel, our deterministic algorithm to enumerate the samples per pixel starts by selecting the resolution of the Hilbert curve (see Fig. 1) to match the image resolution. We therefore determine the smallest power of two that is larger or equal to the maximum of the image resolution in horizontal and vertical direction. Enumerating the pixels along the Hilbert curve, for each pixel we draw the selected samples from the low discrepancy sequence in contiguous blocks. Pixels outside the image are simply skipped.

As shown in Fig. 5, this simple algorithm performs astonishingly well in comparison to using the first two dimensions of the same low discrepancy sequence to sample the pixels of the image mapped to the unit square [12]. While both approaches expose about the same ℓ^2 -error as argued in [10], sampling along the Hilbert curve

results in noise that is much more uniformly distributed across the image, especially visible at low sampling rates.

The human visual system always tries to detect scale invariant features and unfortunately finds such in the non-uniformities of noise, too. As such features are not related to the actual image content, they are perceived as disturbing artifacts. If, however, the noise is uniform it is less likely misinterpreted and consequently noise is not perceived as much. As a result, one may argue that the eye is filtering the noise by integrating over areas of uniform noise in the image. While the blue noise sampling approaches mentioned in the previous section rely on this phenomenon, our new approaches are deterministic and do not require optimization.

Enumerating low discrepancy sequences along space filling curves by spatial proximity [29] suggests that contiguous blocks of samples from a low discrepancy sequence are spatially close and hence improve local uniformity. Similarly, using a variant of the Morton curve (see Fig. 1) combined with scrambling to enumerate pixels [2] results in an error more uniformly distributed across the image. The observable improvements are supported by the fact that the low discrepancy of a point sequence is preserved when enumerated along the Hilbert curve [11]. In addition, we can adopt an argument from [21, Sec.3.2]: Considering an image as a line of pixels as enumerated along the Hilbert curve and assuming the function to be integrated along the pixel to have a gradient bounded by K , the total variation is bounded by K times the length of the Hilbert curve, which in turn bounds the integration error by the Koksma-Hlawka inequality [23]. While the Hilbert, Moore, or Peano curve achieve a shortest route to connect all pixels, the Morton curve fails to do so, which explains parts of its inferiority. On a historical note, both [29] and [2] mention the Hilbert curve but used the Morton curve and hence cannot not take advantage of the above argument. As compared to the Morton and Peano curve, both the Hilbert and Moore curve expose a smaller maximum number of curves segments in the 3×3 neighborhood of a pixel (see Fig. 1), resulting in more consecutive samples of the low discrepancy sequence in the neighborhood, which improves uniformity locally.

In computer graphics gradients may be bounded in parts of the integration domain, however, such parts usually cannot be identified efficiently. Yet, Fig. 5 clearly shows that in such smoother regions of an image the noise is much more uniformly distributed when using the proposed algorithm. The human visual system takes advantage of these local improvements.

3.1 Correlation in Space-Filling Curves

We show that the correlation patterns visualized in Fig. 2 emanate from enumerating radical inverses [23] along a space-filling curve. A radical inverse

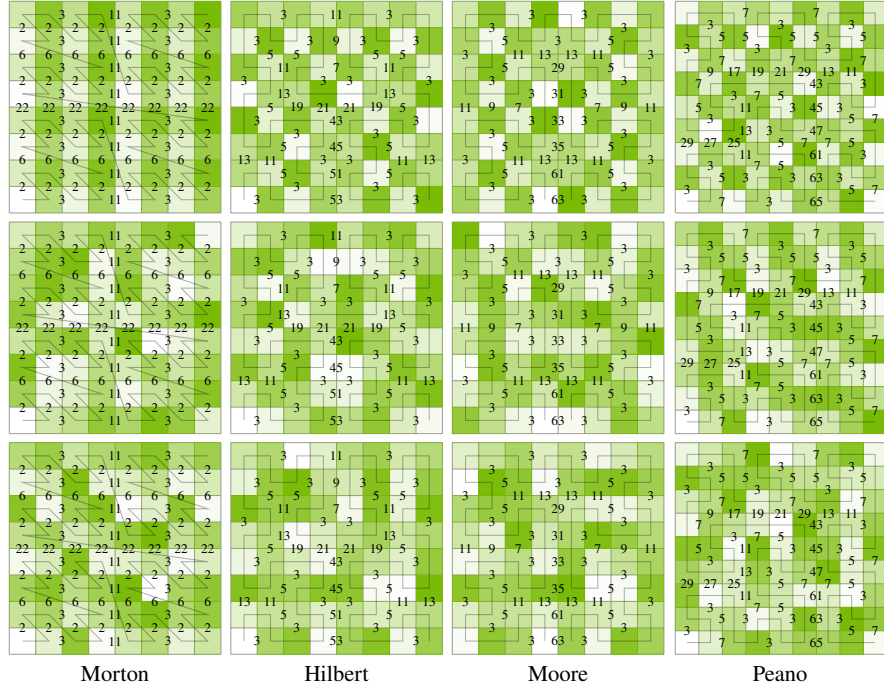


Fig. 2 The numbers on the edges shared by neighboring pixels are the difference of pixel indices enumerated along the depicted space-filling curve. Along the curve, this difference is one and implicitly represented by the imprinted curves. Diagrams in a column belong to the named space-filling curve. From top to bottom, the rows show the differences for the radical inverses ϕ_2 , ϕ_3 , and ϕ_5 , while the shade of each pixel represents the value of the radical inverse of the pixel index. As can be seen, the differences contain symmetries and repetitive patterns, which result in visible correlations in the pixels shades. For curves in base $b = 2$, it is easy to spot a checker-boarding effect. For the Peano curve, symmetries along the diagonal may be observed. Besides this illustration of the principle, structures may be more visible at higher resolutions, see Fig. 3

$$\begin{aligned} \phi_b : \mathbb{N}_0 &\rightarrow \mathbb{Q} \cap [0, 1) \\ i = \sum_{k=0}^{\infty} a_k(i) b^k &\mapsto \sum_{k=0}^{\infty} a_k(i) b^{-k-1} \end{aligned} \quad (1)$$

maps a non-negative integer to the unit interval by reflecting its digits $a_k(i)$ in base b at the decimal point. The Halton sequence is an example of an infinite-dimensional low discrepancy sequence. Each dimension is a radical inverse, where all the bases are relatively co-prime. The uniformity of the simple construction can be improved by applying a permutation to the k -th digit $a_k(i)$ of the index i represented in base b before radical inversion. Zaremba [31] has been successful with the simple permutation $\pi_b(a_k(i)) := (a_k(i) + k) \bmod b$, while later on Faure [8] developed a more general set of permutations improving upon Zaremba's results.

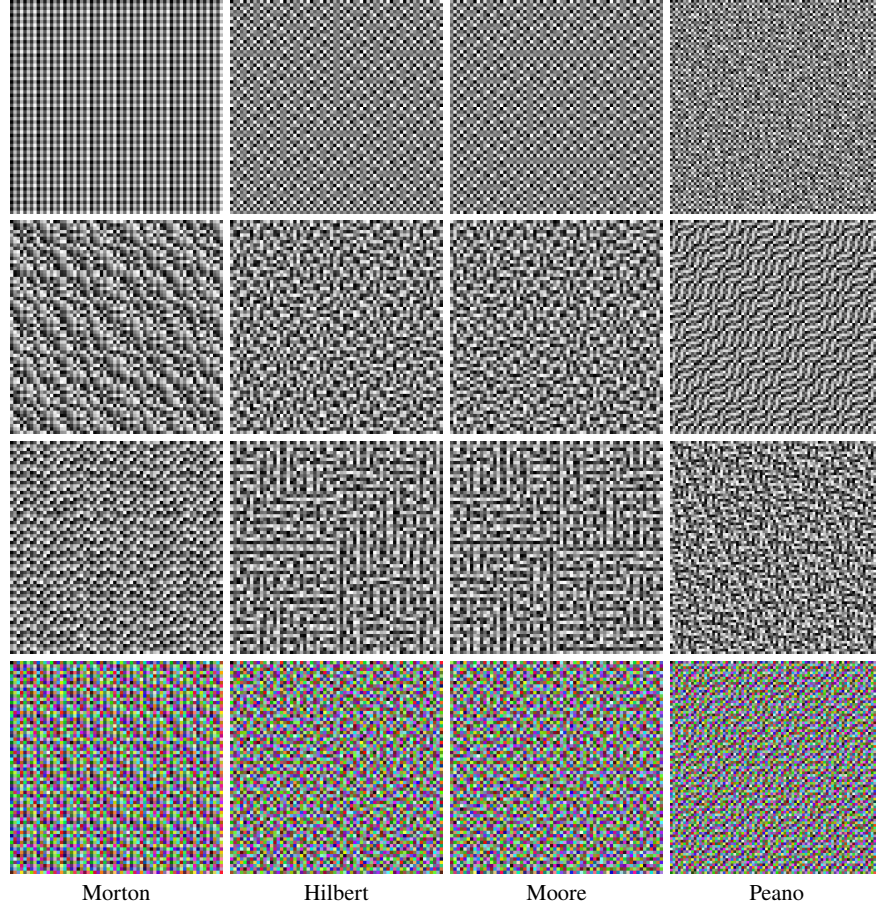


Fig. 3 From top to bottom, the rows display the values of the radical inverses ϕ_2 , ϕ_3 , and ϕ_5 as gray values, and all previous three superimposed by assigning them to the RGB channels of an image. The columns indicate the space filling curve used for enumeration. The resolution for the Morton, Hilbert, and Moore curves in base $b = 2$ is 64×64 pixels, while for the Peano curve in base $b = 3$ we display 81×81 pixels. For the eye it is easy to spot regular structures that are caused by correlations between the single low discrepancy sequences and the space filling curves. Superimposing them as in the bottom row, it becomes harder to identify the correlations with the Moore and Hilbert curves.

Now taking a look at the Morton curve in Fig. 2, it becomes obvious that the Morton index is either odd or even per column of pixels. As a consequence, computing the radical inverse ϕ_2 of this index, which amounts to bits reversal of the index, results in $\phi_2 < \frac{1}{2}$ in even columns and $\phi_2 \geq \frac{1}{2}$ in odd columns [2, Sect.3.1]. Similarly, the second least significant bit of the Morton index is on and off along the rows of pixels. This correlation results in striping artifacts along rows and columns of pixels, especially visible at one sample per pixel as shown in Fig. 3.

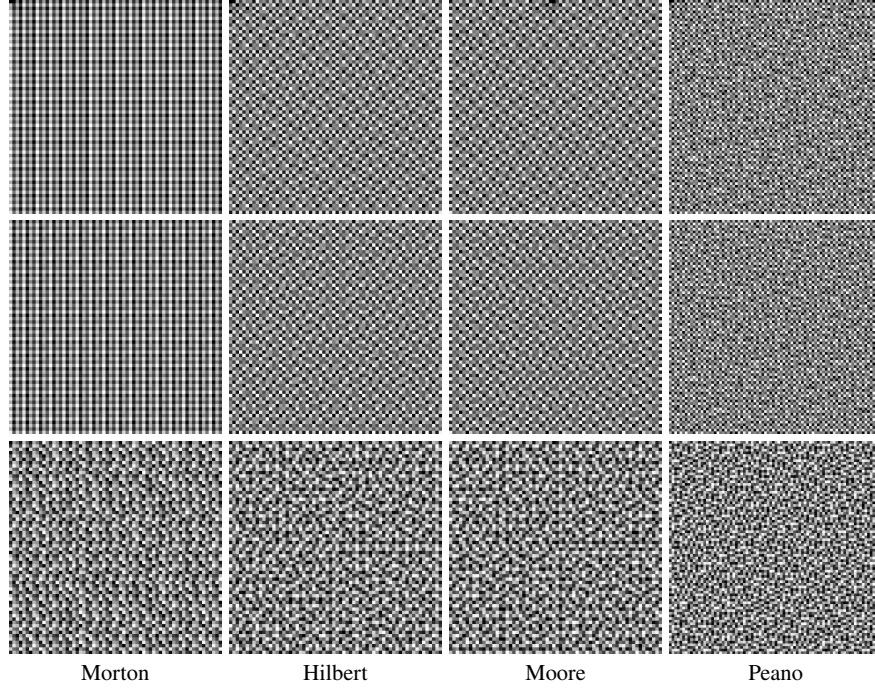


Fig. 4 While scrambling may attenuate visible correlations between pixels, it cannot completely remove the correlations. The first row shows ϕ_2 with random digit scrambling and the second row shows ϕ_2 with Owen scrambling. The bottom row shows ϕ_5 improved according to Faure [9]. As compared to Fig. 3, scrambling ϕ_2 does not at all help when used with the Morton curve and still leaves some visible lines indicative of the quadrant structure of the Hilbert and Moore curves. For the example of ϕ_5 , scrambling helps most for the correlations when using the Peano curve but does not dramatically attenuate the artifacts when using the other space filling curves.

Other space-filling curves expose correlations, too, the reason being simply that the differences of indices of pixels are deterministic and correlated. Fig. 2 shows the index differences larger than one for neighboring pixels. While the Hilbert and Moore curves are in base $b = 2$, they expose correlations with ϕ_3 and higher bases. For example, stripes are visible along lines of differences that are a multiple of the radical inverses' base 3. Similarly, the Hilbert curve has many adjacent pairs of pixels, whose difference of indices is 3. Radical inverses in these pixels in base $b = 3$ hence are correlated. The larger such clusters, the more prominent is the visible artifact.

While correlations are to be expected when the base of the low discrepancy sequence and the space filling curve are not co-prime, correlation structures may become visible whenever the differences of the pixel indices along a space filling curve are correlated to the base of the low discrepancy sequence in a regular way.

Owen scrambling [24] may resolve these correlations, because it recursively partitions the unit interval and randomly swaps the partitions independently. For the

case of the Morton curve, Ahmed [2] developed a scrambling scheme, where it is sufficient to apply the recursive random swapping procedure to the index of the pixel along the Morton curve. The algorithm amounts to applying random permutations to the contiguous block of indices belonging to each quadrant along the hierarchy of the Morton curve.

As exemplified in Fig. 4, even recursive scrambling cannot remove all correlation artifacts. For example, in base $b = 2$, the recursive structure of scrambling correlates with the block structure of the Morton, Moore, and Hilbert curves. Yet, visible correlation artifacts are attenuated. Note that for the most significant bit both digit scrambling and Owen scrambling are identical. No matter how or whether this bit is scrambled, consecutive pixels along a space filling curve are hence larger and less or equal to $\frac{1}{2}$. In contrast to the Morton curve, this guarantees a good uniformity of values in the neighborhood of each pixel for the Hilbert, Moore, and Peano curves. For the example of base $b = 5$, scrambling may attenuate the visible structures and yet cannot resolve the correlations of the base of the radical inverse and the difference of pixel indices as shown in Fig. 2.

3.2 Blue-Noise Dithered Sampling

While some correlations are visible in low dimensions and at low sampling rates, sampling light transport paths requires many more dimensions. Fig. 3 illustrates that already overlaying the first three radical inverses as RGB values hides most of the disturbing artifacts.

The maps in Fig. 3 resemble the maps used for blue-noise dithered sampling [10] and may be used for the same purposes. As opposed to the optimization process required to create blue-noise dither maps, enumerating low discrepancy sequences along a space-filling curve allows one to approximate the desired spectral properties by just selecting components without the restriction to low dimension and without the need to store lookup tables. This approach is partially explored in Sect. 4.1.

4 Progressive Image Synthesis

Progressive image synthesis continues sampling within a given sample or time budget or terminates sampling once a selected image quality has been reached [19]. In what follows, we discuss extensions of the consistent algorithm of the previous section to enable adaptive sampling.

4.1 Deterministic Cranley-Patterson Rotation

Similar to the algorithm detailed in Sect. 3, a low discrepancy sequence is enumerated along the Hilbert curve at one sample per pixel. The vector of the low discrepancy sequence assigned to a pixel then is used to perform a deterministic Cranley-Patterson rotation [6]. This way, the same sequence of samples may be used across all pixels, however, shifted individually.

The Cranley-Patterson rotation is implemented as component-wise addition modulo one. Yet, using one and the same low discrepancy sequence for both shifting and sampling may expose visible correlation artifacts at low sampling rates. This is the case when enumerating the improved Halton sequence [9] along the Hilbert curve to shift the same sequence per pixel. While Cranley-Patterson rotations work with any point set, they work best with a point set designed for the unit torus such as rank-1 lattices and rank-1 lattice sequences [14]. For results, see Fig. 5.

4.2 Randomization

Array-RQMC algorithms [21] randomize the low discrepancy sequence for each iteration. This approach is straightforward to apply to the algorithm in Sect. 3: for each pass, the low discrepancy sequence is randomized and the results are accumulated until the termination by an empirical error criterion is triggered or a given time budget expired. The repeated randomization will eventually average out the correlation artifacts in the rendered frame.

While randomizing the low discrepancy sequence and accumulating results is unbiased and allows for unbiased variance estimation, some uniformity and hence convergence speed is sacrificed. Therefore, we aim at a deterministic and consistent algorithm, which in addition is simpler to execute and reproduce on massively parallel computer systems [15, 19].

4.3 Contiguous Segments of one Low Discrepancy Sequence

Progressive sampling may be implemented by iterating the algorithm in Sect. 3. To increase the uniformity of the samples in a pixel, one approach is to double the sampling rate with each iteration. Randomizing the low discrepancy sequence freshly for each iteration, the scheme is unbiased, see Sect. 4.2.

A deterministic variant of the algorithm sequentially consumes the points of the low discrepancy sequence along the space filling curve according to the selected number of samples per pixel along the iterations. The segment lengths drawn from the sequence then are a multiples of the length of the selected space filling curve. In two dimensions, the length is a quadratic power of the base of the selected space-filling curve.

For the example of base two, segment lengths amount to multiples of powers of two. Hence, for a specific pixel, samples drawn from a radical inverse in base $b = 2$ are spaced in multiples of powers of two, which will reveal correlation artifacts as visualized in Fig. 2. Depending on the combination of space filling curve and component of the low discrepancy sequence, samples may even not be distributed uniformly, as explained in Sect. 3.1. Omitting the components of the low discrepancy sequence that correlate with the space-filling curve may help, but as revealed in Sect. 3.1, there may be multiple components with correlations.

The issues of leapfrogging low discrepancy sequences have been encountered in parallelizing quasi-Monte Carlo methods [20, 1]. Their remedy has led to the concept of partitioning low discrepancy sequences into multiple low discrepancy sequences, which we explore next.

4.4 Partitioning one Low Discrepancy Sequence

Partitioning a low discrepancy sequence into a finite number of low discrepancy sequences has been introduced in [18] for the purpose of parallel quasi-Monte Carlo methods: One dimension of a low discrepancy sequence is used for partitioning, while the remaining dimensions are used for quasi-Monte Carlo integration. We use the principle to develop a simple consistent algorithm for rendering along the Hilbert curve.

Let $\phi_b(i)$ be the component of a low discrepancy sequence to be partitioned into $N = b^m$ low discrepancy sequences and let \mathbf{x}_i be the points of that low discrepancy sequence without the component used for partitioning. Then the integers

$$\lfloor N \cdot \phi_b(i) \rfloor = \lfloor b^m \cdot \phi_b(i) \rfloor = \left\lfloor b^m \cdot \sum_{k=0}^{\infty} a_k(i) b^{-k-1} \right\rfloor,$$

form a permutation of $\{0, \dots, N-1\}$ that repeats every N points. Selecting N as the length of a space filling curve and b its base, each pixel with index j along the space-filling curve is assigned the sequence of points

$$P_j = \left\{ \mathbf{x}_{l \cdot N + \phi_b^{-1}(j/N)} : l \in \mathbb{N}_0 \right\} \Leftrightarrow P_{\phi_b^{-1}(j/N)} = \left\{ \mathbf{x}_{l \cdot N + j} : l \in \mathbb{N}_0 \right\}$$

of the original low discrepancy sequence \mathbf{x}_i , which results in an overall consistent deterministic quasi-Monte Carlo method [15, Sect.1.1].

As the offset $\phi_b^{-1}(j/N)$ is constant per pixel, omitting the inverse of the permutation $\lfloor b^m \cdot \phi_b(i) \rfloor$ and instead assigning

$$P_j = \left\{ \mathbf{x}_{l \cdot N + j} : l \in \mathbb{N}_0 \right\}$$

simplifies the implementation: Now contiguous blocks of the low discrepancy sequence are enumerated along the space-filling curve and we have the additional

benefit of locally improved uniformity as described in Sect. 3 and illustrated in Fig. 1.

For the combination of the Hilbert curve and the improved Halton sequence [9] for progressive image synthesis, we have $b = 2$ and use ϕ_2 to partition the low discrepancy sequence into $N = 2^{2n}$ low discrepancy sequences, one for each pixel along the Hilbert curve. The algorithm uses the pixel index j along the Hilbert curve as offset into the low discrepancy sequence \mathbf{x}_i and leapfrogs from there with a stride of N , which is simple to execute on a massively parallel computer system, like for example a GPU cluster [18, 19, 3].

5 Results and Discussion

The Hilbert curve has been applied in computer graphics before. Rendering images by enumerating pixels along the Hilbert curve improves performance by higher cache hit rates due to the locality properties of the Hilbert curve. The visual benefits of half-toning by dithering along the Hilbert curve have been recognized in [28].

Our new algorithms benefit from these findings. They are a special case of Array-RQMC that does not require sorting, as we rely on the bijection between pixels and the space-filling curves. As indices can be computed directly, neither lookup tables nor additional memory for lookup tables are required.

Our focus is on deterministic algorithms, as these can be reliably parallelized and results are exactly reproducible [15]. We use an improved variant of the Halton sequence [9] in the experiments. The implementation of fitting elementary intervals to the pixel raster [12] is involved and requires 64-bit signed integers to run Euclid's algorithm for the Chinese remainder theorem. This computation is not required for the algorithms in Sect. 3 and Sect. 4.4 that are straightforward to implement. Shifting a rank-1 lattice sequence [14] by the Halton sequence enumerated along the Hilbert curve (see Sect. 4.1) is even simpler and practical with only two 32-bit integer indices. We employ an extensible lattice constructed by primitive polynomials [16]. To assess the visual differences of the classic [12] and the two new progressive sampling approaches, their results are compared at low sampling rates in Fig. 5.

The most prominent advantage of the new algorithms is inherited from Array-RQMC: As illustrated in Fig. 1, the Hilbert curve has the smallest number of curve segments in the neighborhood around a pixel. Hence more consecutive samples are used locally, which makes better use of the uniformity of a low discrepancy sequence across pixels as compared to other space-filling curves. Hence, the noise in the images is more uniformly distributed noise at low sampling rates.

Our methods achieve a quality comparable to methods that require optimization [10, 13], are available for any number of dimensions, are simpler than other approaches that sample along space-filling curves [2], are deterministic, and are consistent.

We have not yet explored the potential of selecting or reordering the dimensions of low discrepancy sequences. This is an interesting direction of future research that has

been initially explored for rank-1 lattices in computer graphics [22]. Furthermore, it is worth investigating the many other possible combinations of low discrepancy sequences and space-filling curves with respect to their visual quality and convergence speed.

6 Conclusion

Based on the seminal work on Array-RQMC [21], we introduced simple deterministic consistent rendering algorithms that at low sampling rates produce noise characteristics that are very amenable to the human eye. Key to the algorithms are the preservation of discrepancy when enumerating low discrepancy sequences along the Hilbert curve and the principle of partitioning one low discrepancy sequence into multiple. It appears that the correlation of samples across pixels via low discrepancy may be more relevant to the eye than their independence.

References

1. Abramov, G.: US patent #6,911,976: System and method for rendering images using a strictly-deterministic methodology for generating a coarse sequence of sample points (2002). Assignee: mental images GmbH (Berlin, DE)
2. Ahmed, A.G.M., Wonka, P.: Screen-space blue-noise diffusion of Monte Carlo sampling error via hierarchical ordering of pixels. *ACM Trans. Graph.* **39**(6) (2020). DOI 10.1145/3414685.3417881. URL <https://doi.org/10.1145/3414685.3417881>
3. van Antwerpen, D., Seibert, D., Keller, A.: A simple load-balancing scheme with high scaling efficiency. In: E. Haines, T. Akenine-Möller (eds.) *Ray Tracing Gems*. Apress (2019). <http://raytracinggems.com>
4. Binder, N., Fricke, S., Keller, A.: Massively parallel path space filtering. In: A. Keller (ed.) *Monte Carlo and Quasi-Monte Carlo Methods 2020*. Springer (2022). URL <http://arxiv.org/abs/1902.05942>
5. Cook, R.L.: Stochastic Sampling in Computer Graphics. *ACM Transactions on Graphics* **5**, 51–72 (1986)
6. Cranley, R., Patterson, T.: Randomization of number theoretic methods for multiple integration. *SIAM Journal on Numerical Analysis* **13**, 904–914 (1976)
7. Ernst, M., Stamminger, M., Greiner, G.: Filter importance sampling. In: *Proc. 2006 IEEE/EG Symposium on Interactive Ray Tracing*, pp. 125–132 (2006)
8. Faure, H.: Good permutations for extreme discrepancy. *J. Number Theory* **42**, 47–56 (1992)
9. Faure, H., Lemieux, C.: Improved Halton sequences and discrepancy bounds. *Monte Carlo Methods Appl.* **16**(3-4), 231–250 (2010). DOI 10.1515/mcma.2010.008. URL <https://doi.org/10.1515/mcma.2010.008>
10. Georgiev, I., Fajardo, M.: Blue-noise dithered sampling. *ACM SIGGRAPH 2016 Talks* (2016)
11. Gerber, M., Chopin, N.: Sequential quasi Monte Carlo. *Journal of the Royal Statistical Society. Series B (Statistical Methodology)* **77**(3), 509–579 (2015). URL <http://www.jstor.org/stable/24774819>
12. Grünshloß, L., Raab, M., Keller, A.: Enumerating quasi-Monte Carlo point sequences in elementary intervals. In: L. Plaskota, H. Woźniakowski (eds.) *Monte Carlo and Quasi-Monte Carlo Methods 2010*, pp. 399–408. Springer (2012). URL <http://gruenschloss.org/sample-enum/sample-enum.pdf>



Fig. 5 Photorealistic image synthesis using one low discrepancy sequence across the image plane (left column, [12]), drawing samples from one low discrepancy sequence while enumerating the pixels along the Hilbert curve to shift an extensible lattice for sampling inside a pixel (middle column, Sect. 4.1) and in contiguous blocks to directly sample inside a pixels (right column, Sect. 4.4). The top image has been rendered using 100,000 samples per pixel, while the insets from top to bottom were rendered at 1, 4, 16, and 64 samples per pixel, respectively. The more uniformly distributed and less splotchy appearance of the sampling noise is especially visible in areas that at higher sampling rates appear smooth, like the table top or the back rests. The difference in quality is clearly visible on a computer screen and may be difficult to reproduce in print. The reader may need to vary the distance of observation. As all methods are consistent, the observable differences vanish with an increasing number of samples per pixel. Nevertheless, the improvement very much matters in settings, where only a small number of samples are affordable, such as in real-time rendering.

13. Heitz, E., Belcour, L., Ostromoukhov, V., Coeurjolly, D., Iehl, J.C.: A low-discrepancy sampler that distributes Monte Carlo errors as a blue noise in screen space. In: SIGGRAPH'19 Talks. ACM, Los Angeles, United States (2019). URL <https://hal.archives-ouvertes.fr/hal-02150657>
14. Hickernell, F., Hong, H., L'Ecuyer, P., Lemieux, C.: Extensible lattice sequences for quasi-Monte Carlo quadrature. *SIAM J. Sci. Comput.* **22**, 1117–1138 (2001)
15. Keller, A.: Quasi-Monte Carlo image synthesis in a nutshell. In: J. Dick, F. Kuo, G. Peters, I. Sloan (eds.) *Monte Carlo and Quasi-Monte Carlo Methods 2012*, pp. 203–238. Springer (2013)
16. Keller, A., Binder, N., Wächter, C.: Construction of a rank-1 lattice sequence based on primitive polynomials. In: G. Larcher, F. Pillichshammer, A. Winterhof, C. Xing (eds.) *Applied Algebra and Number Theory*, pp. 204–215. Cambridge University Press (2014). DOI 10.1017/CBO9781139696456.013
17. Keller, A., Georgiev, I., Ahmed, A., Christensen, P., Pharr, M.: My favorite samples. In: ACM SIGGRAPH 2019 Courses, SIGGRAPH '19, pp. 15:1–15:271. ACM, New York, NY, USA (2019). DOI 10.1145/3305366.3329901. URL <http://doi.acm.org/10.1145/3305366.3329901>
18. Keller, A., Grünschloß, L.: Parallel quasi-Monte Carlo integration by partitioning low discrepancy sequences. In: L. Plaskota, H. Woźniakowski (eds.) *Monte Carlo and Quasi-Monte Carlo Methods 2010*, pp. 487–498. Springer (2012). URL <http://gruenschloss.org/parqmc/parqmc.pdf>
19. Keller, A., Wächter, C., Raab, M., Seibert, D., Antwerpen, D., Korndörfer, J., Kettner, L.: The Iray light transport simulation and rendering system. *CoRR* **abs/1705.01263** (2017). URL <http://arxiv.org/abs/1705.01263>
20. Kocis, L., Whiten, W.: Computational investigations of low-discrepancy sequences. *ACM Trans. Math. Softw.* **23**(2), 266–294 (1997). DOI <http://doi.acm.org/10.1145/264029.264064>
21. L'Ecuyer, P., Munger, D., Lécot, C., Tuffin, B.: Sorting methods and convergence rates for Array-RQMC: Some empirical comparisons. In: *Mathematics and Computers in Simulation*, vol. 143 (2018)
22. Liu, H., Han, H., Jiang, M.: Rank-1 lattices for efficient path integral estimation. *Computer Graphics Forum* **40**(2), 91–102 (2021). DOI <https://doi.org/10.1111/cgf.142617>. URL <https://onlinelibrary.wiley.com/doi/abs/10.1111/cgf.142617>
23. Niederreiter, H.: *Random Number Generation and Quasi-Monte Carlo Methods*. SIAM, Philadelphia (1992)
24. Owen, A.: Randomly permuted (t, m, s) -nets and (t, s) -sequences. In: H. Niederreiter, P. Shiu (eds.) *Monte Carlo and Quasi-Monte Carlo Methods in Scientific Computing, Lecture Notes in Statistics*, vol. 106, pp. 299–315. Springer (1995)
25. Paulin, L., Coeurjolly, D., Bonneel, N., Iehl, J.C., Keller, A., Ostromoukhov, V.: Matbuilder: Mastering sampling uniformity over projections. *ACM Transactions on Graphics* **41**(4), xx:1–xx:13 (2022)
26. Paulin, L., Coeurjolly, D., Iehl, J.C., Bonneel, N., Keller, A., Ostromoukhov, V.: Cascaded Sobol' sampling. *ACM Transactions on Graphics* **40**(6), 274:1–274:13 (2021). URL <https://hal.archives-ouvertes.fr/hal-03358957>
27. Pharr, M., Jacob, W., Humphreys, G.: *Physically Based Rendering - From Theory to Implementation*. Morgan Kaufmann, Third Edition (2016)
28. Velho, L., Gomes, J.d.M.: Digital halftoning with space filling curves. In: *Proceedings of the 18th Annual Conference on Computer Graphics and Interactive Techniques, SIGGRAPH '91*, p. 81–90. Association for Computing Machinery, New York, NY, USA (1991). DOI 10.1145/122718.122727. URL <https://doi.org/10.1145/122718.122727>
29. Wächter, C., Keller, A.: Efficient simultaneous simulation of Markov chains. In: A. Keller, S. Heinrich, H. Niederreiter (eds.) *Monte Carlo and Quasi-Monte Carlo Methods 2006*, pp. 669–684. Springer (2007)
30. Yellot, J.: Spectral Consequences of Photoreceptor Sampling in the Rhesus Retina. *Science* **221**, 382–385 (1983)

31. Zaremba, S.: La discr pance isotrope et l'int gration num rique. *Ann. Mat. Pura Appl.* **87**, 125–136 (1970)